Supporting information

Materials and methods

Experimental

Complex $[Y(pc)_2]^{\bullet}$ was prepared by a previously reported method.[1] X-ray diffraction data were collected on a Bruker D8 diffractometer using monochromatic Cu-Ka (λ = 1.540600 Å) radiation with a scanning range between 4 and 40° and a scan rate of 1.60°min^{-1}.

The EPR sample (10 mg) was evacuated for 30 min in the EPR tube and then flame-sealed under a helium atmosphere. The same sample was used for RT-CW and pulse experiments giving strong signals in both cases, though precise comparison of the intensities was not attempted as the task was complicated by the fact that experiments were run on different resonators and spectrometers. For 5 K CW studies, a smaller sample was prepared, as the signal strength perturbed the cavity.

CW EPR spectra at the X-band (9.3 GHz) were collected on an EMXplus spectrometer fitted with an EMX microX bridge and a Bruker ER4122SHQE cavity operating in the TE_{011} mode.

Pulsed EPR spectra were collected at the X-band (9.7 GHz) on a Bruker ELEXSYS E580 spectrometer, fitted with an upgraded ESP1010 microwave bridge and a Bruker EN 4118X-MD4 pulse-ENDOR resonator. For low-temperature experiments the resonator was fitted in an Oxford CF935 dynamic continuous flow cryostat and the temperature was regulated with an Oxford Mercury iTC.

FIDs ($\pi/2 - t_d$ – FID) were collected after a $\pi/2$ pulse, of accordingly adjusted length and power. The dead time t_d was ~600 ns. Inversion-recovery ($\pi - t - \pi/2 - t_d$ – FID) and nutation ($t_{nut} - t_d$ – FID) experiments were conducted with a 400 ns integration window. For FID-detected field-swept spectra, the FIDs were collected at different fields and integrated. Different pulse selectivities were obtained by properly adjusting the pulse lengths and the MW power.

FIDs were fitted with the exponential decay function $M(t) = M_0 e^{-(t/T_m)}$ and inversion-recovery traces were fitted with the stretched exponential function $M(t) = M_\infty - 2M_0 e^{-(t/T_1)^\beta}$.

Prior to Fourier transforms, nutation traces were baseline-corrected with a symmetric Huber function, zero-filled to double the datasets' initial lengths (from 512 to 102 points), and apodized with a Chebysev or Hamming window function. Each spectrum was normalized with respect to its maximum intensity, which was set to unity.

Calculations

We performed periodic calculations using the Gaussian-Planewave code CP2K.[2–5]. To take into account the exchange and correlation contributions to the total energy the Meta-GGA functional TPSS (Tao-Perdew-Staroverov-Scuseria)[6] was used in all spin polarised calculations. Molecule Optimized Triple Zeta Basis functions[7] were chosen for the valence electrons while GTH Pseudopotentials[8,9] to consider the core electrons.

Two types of simulation boxes were used to analyse the different spin multiplicities. The first set of parameters were provided by the VUKZAD[10] dataset and have as lattice vectors: a = 8.835, b = 10.616 and c = 50.789 Å and $\alpha = \beta = \gamma = 90°$. This lattice parameters correspond to a perfect lattice consisting on periodically repeated $[YPc_2]$ molecules. For the second simulation box, the

angles remained the same while the lattice constants were set to: a = 60.0, b = 30.0 and c = 30.0 Angstroms.

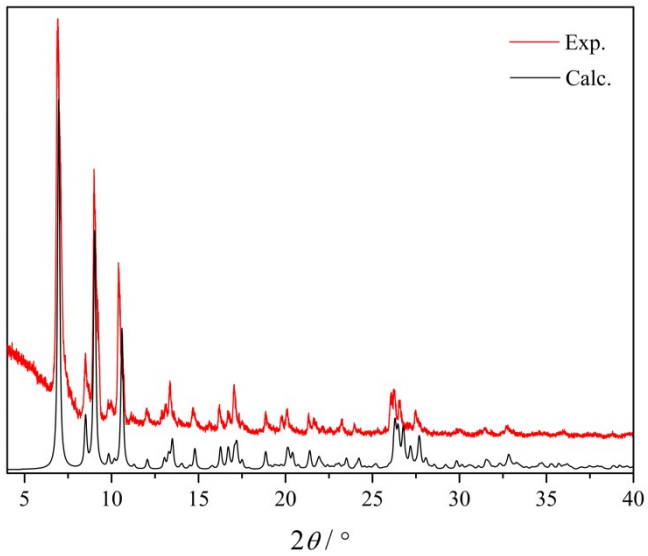

Figure S1. Room-temperature powder XRD diffractogram of the [Y(pc)$_2$] sample (red line). The calculated diffractogram (black line) is based on the single-crystal structure collected at 93 K (CCDC code: VUKZAD).

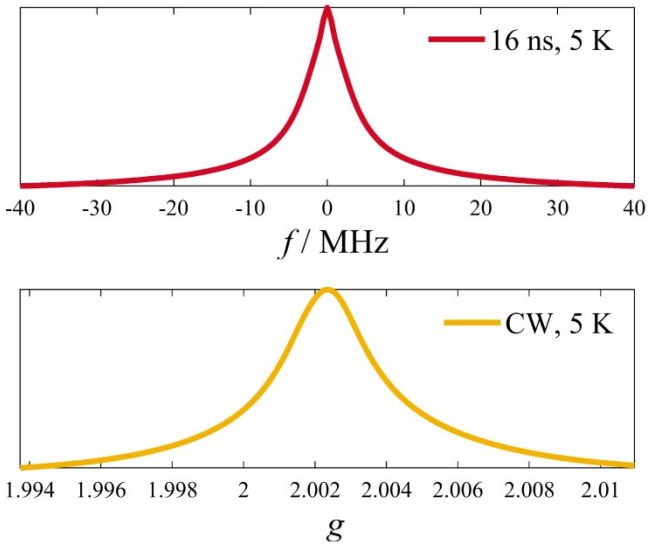

Figure S2. FID-detected EPR spectra of [Y(pc)$_2$]$^{\bullet}$ at 5 K (top) compared to the CW spectrum plotted in absorption mode (bottom). The g-scale is plotted from the H-scale derived by considering a 2.80 MHz/G correspondence. Exp. Conditions. CW spectrum: f_{MW} = 9.31051 GHz, ΔB_{mod} = 0.1 G_{pp}, P_{MW} = 0.606 mW. Pulsed spectrum: f_{MW} = 9.73914 GHz

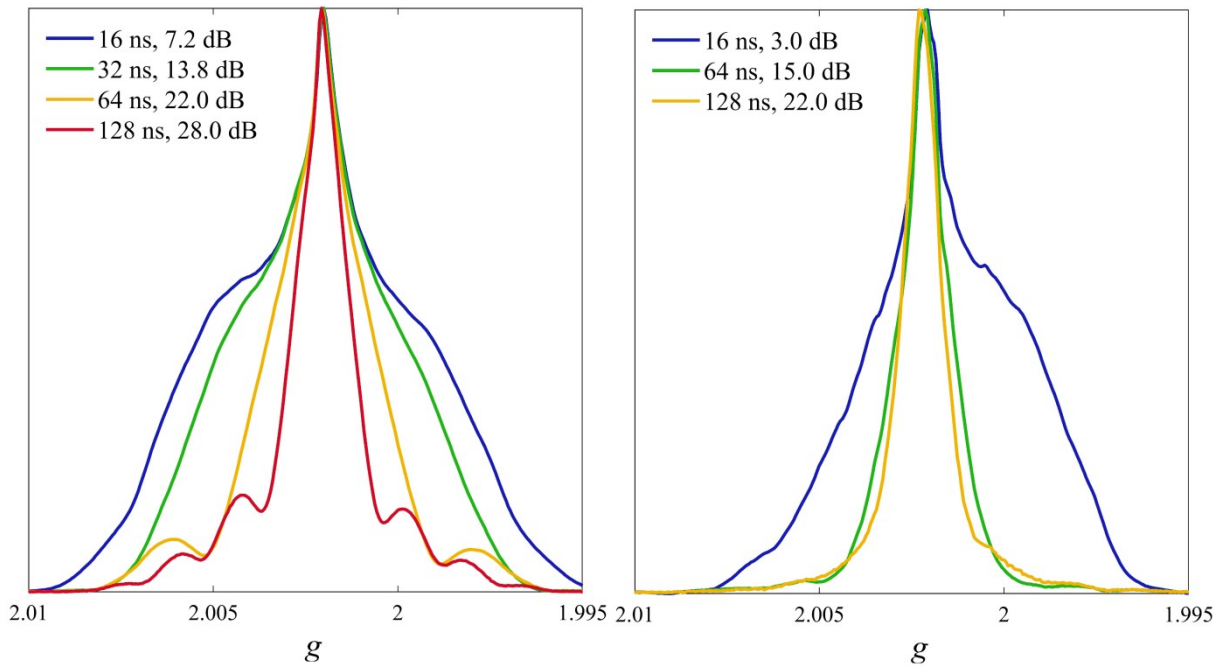

Figure S3. FID-detected field-swept EPR spectra at 295 K (left) and 5 K (right) with pulses of varying selectivities.

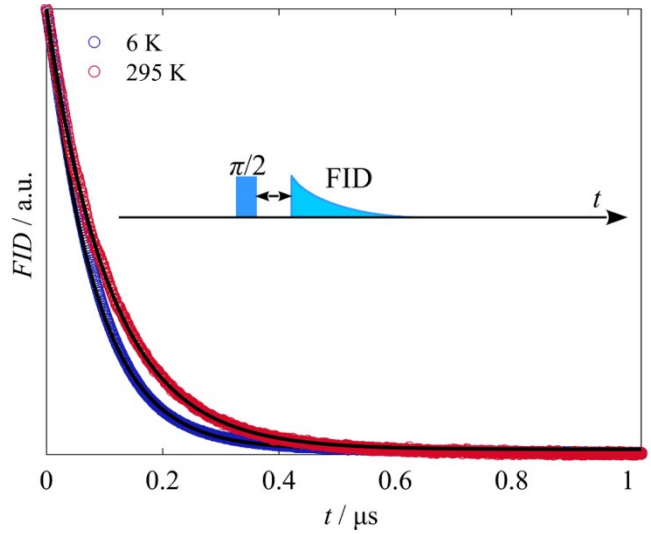

Figure S4. FID of $[Y(pc)_2]$ at resonance. The inset shows the pulse sequence. The double-headed arrow indicates the dead time.

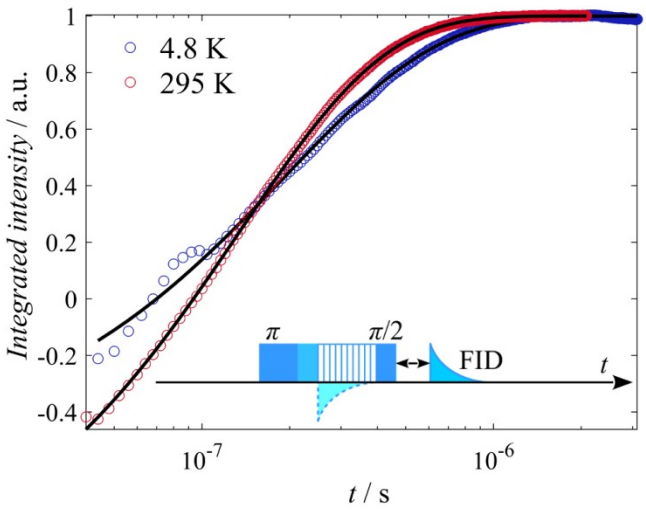

Figure S5. Inversion-recovery traces and fits. The inset shows the pulse sequence. The double-headed arrow indicates the dead time.

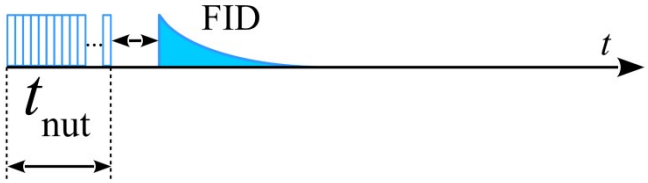

Figure S6. Pulse sequence for FID-detected nutation experiments. The double-headed arrow indicates the dead time.

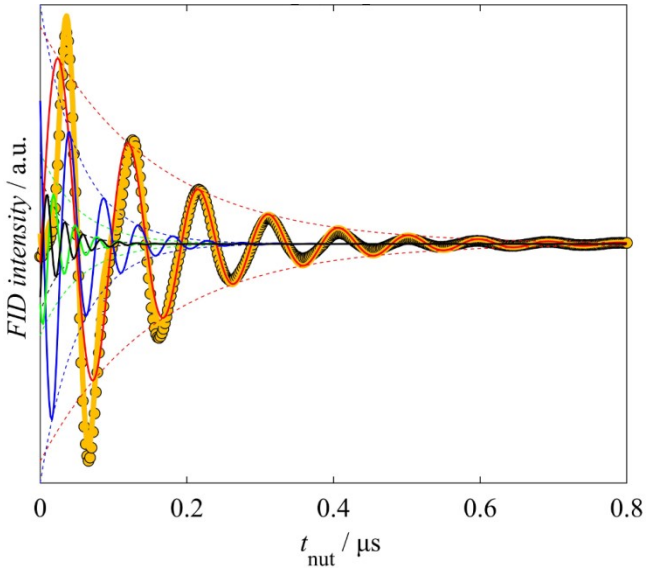

Figure S7. Rabi oscillations at 5 K, at 10 dB microwave power attenuation. The thin solid lines are the exponentially damped oscillations of frequencies f_1 (= 10.46 MHz, red), $2f_1$ (blue), $3f_1$ (green) and $4f_1$ (black). The thin dashed lines of the same colors are the exponential decay envelopes for each of the oscillations.

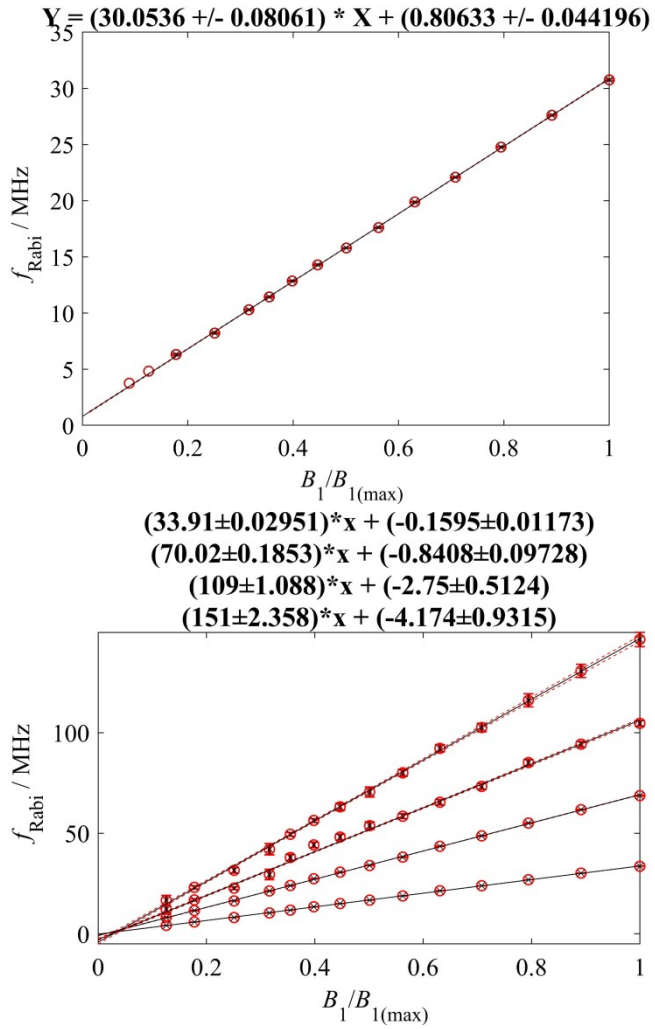

Figure S8. Linear Deming fits of the 295 K (top) and 5 K (bottom) MW power dependence of the Rabi frequencies derived from fits to the nutation traces. The error bars correspond to the 1σ confidence intervals of each fitted value.

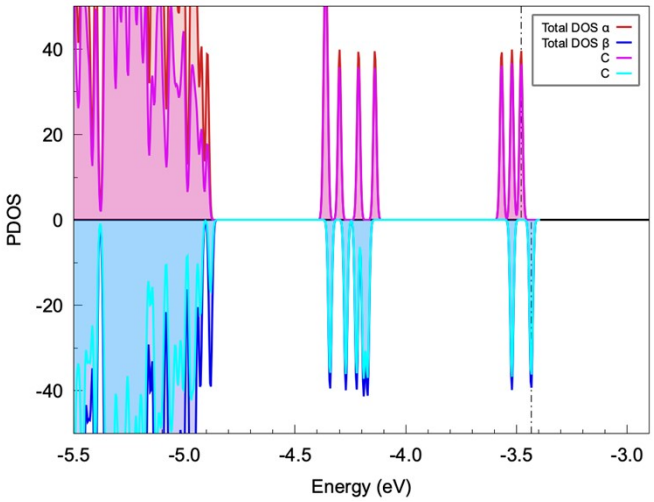

Figure S9. Projected density of states of the 5-membered system. As can be clearly seen, the electrons of the ligands are all localised around E = -3.5 eV and correspond to the multiplicity set in the DFT simulations (S_T = 1/2) and the results of the spin density. Practically all spin density is localised on the carbon atoms (magenta and cyan lines).

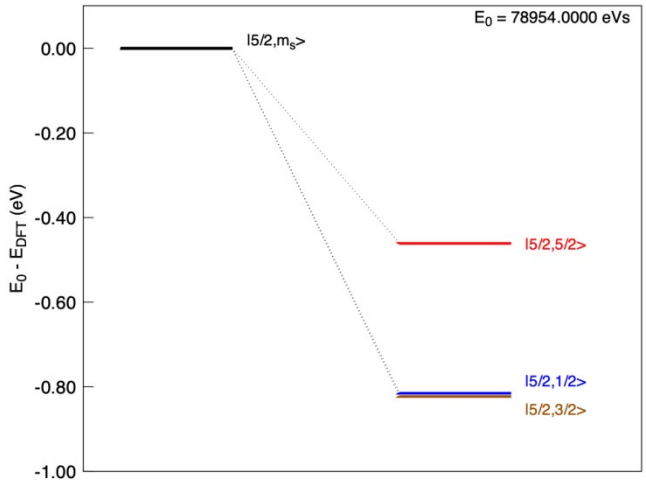

Figure S10. Spin multiplet DFT energies for the m = 5 membered system simulated as a series of $[YPc_2]^{\bullet}$ molecules within a box with empty space between periodic images.

References

1 F. Branzoli, P. Carretta, M. Filibian, M. J. Graf, S. Klyatskaya, M. Ruben, F. Coneri and P. Dhakal, Spin and charge dynamics in $[TbPc_2]^0$ and $[DyPc_2]^0$ single-molecule magnets, *Phys. Rev. B*, 2010, **82**, 134401.

2 G. Lippert, J. Hutter and M. Parrinello, A hybrid Gaussian and plane wave density functional scheme, *Mol. Phys.*, 1997, **92**, 477–487.

3 M. Frigo and S. G. Johnson, The Design and Implementation of FFTW3, *Proc. IEEE*, 2005, **93**, 216–231.

4 J. VandeVondele, M. Krack, F. Mohamed, M. Parrinello, T. Chassaing and J. Hutter, Quickstep: Fast and accurate density functional calculations using a mixed Gaussian and plane waves approach, *Computer Physics Communications*, 2005, **167**, 103–128.

5 J. Hutter, M. Iannuzzi, F. Schiffmann and J. VandeVondele, CP2K: atomistic simulations of condensed matter systems: CP 2 K Simulation Software, *WIREs Comput Mol Sci*, 2014, **4**, 15–25.

6 J. Tao, J. P. Perdew, V. N. Staroverov and G. E. Scuseria, Climbing the Density Functional Ladder: Nonempirical Meta–Generalized Gradient Approximation Designed for Molecules and Solids, *Phys. Rev. Lett.*, 2003, **91**, 146401.

7 J. VandeVondele and J. Hutter, Gaussian basis sets for accurate calculations on molecular systems in gas and condensed phases, *The Journal of Chemical Physics*, 2007, **127**, 114105.

8 C. Hartwigsen, S. Goedecker and J. Hutter, Relativistic separable dual-space Gaussian pseudopotentials from H to Rn, *Phys. Rev. B*, 1998, **58**, 3641–3662.

9 M. Krack, Pseudopotentials for H to Kr optimized for gradient-corrected exchange-correlation functionals, *Theor Chem Acc*, 2005, **114**, 145–152.

10 K. Katoh, Y. Yoshida, M. Yamashita, H. Miyasaka, B. K. Breedlove, T. Kajiwara, S. Takaishi, N. Ishikawa, H. Isshiki, Y. F. Zhang, T. Komeda, M. Yamagishi and J. Takeya, Direct Observation of Lanthanide(III)-Phthalocyanine Molecules on Au(111) by Using Scanning Tunneling Microscopy and Scanning Tunneling Spectroscopy and Thin-Film Field-Effect Transistor Properties of Tb(III)- and Dy(III)-Phthalocyanine Molecules, *J. Am. Chem. Soc.*, 2009, **131**, 9967–9976.